Cancer Research

VHL Gene Mutations and Their Effects on Hypoxia Inducible Factor HIFα: Identification of Potential Driver and Passenger Mutations

Markus P. Rechsteiner[1], Adriana von Teichman[1], Anna Nowicka[1], Tullio Sulser[2], Peter Schraml[1], and Holger Moch[1]

Abstract

Mutations of the von Hippel-Lindau (*VHL*) gene are frequent in clear cell renal cell carcinomas (ccRCC). Nonsense and frameshift mutations abrogate the function of the VHL protein (pVHL), whereas missense mutations can have different effects. To identify those missense mutations with functional consequences, we sequenced *VHL* in 256 sporadic ccRCC and identified 187 different *VHL* mutations of which 65 were missense mutations. Location and destabilizing effects of *VHL* missense mutations were determined *in silico*. The majority of the thermodynamically destabilizing missense mutations were located in exon 1 in the core of pVHL, whereas protein surface mutations in exon 3 affected the interaction domains of elongin B and C. Their impact on pVHL's functionality was further investigated *in vitro* by stably reintroducing *VHL* missense mutations into a *VHL* null cell line and by monitoring the green fluorescent protein (GFP) signals after the transfection of a hypoxia inducible factor (HIF)α-GFP expression vector. pVHL's functionality ranged from no effect to complete HIF stabilization. Interestingly, Asn78Ser, Asp121Tyr, and Val130Phe selectively influenced HIF1α and HIF2α degradation. In summary, we obtained three different groups of missense mutations: one with severe destabilization of pVHL; a second without destabilizing effects on pVHL but relevance for the interaction with HIFα, elongin B, and elongin C; and a third with pVHL functions comparable with wild type. We therefore conclude that the specific impact of missense mutations may help to distinguish between driver and passenger mutations and may explain responses of ccRCC patients to HIF-targeted therapies. *Cancer Res; 71(16); 5500–11. ©2011 AACR.*

Introduction

Renal cell carcinoma (RCC) is the most frequent malignant tumor arising from the kidney with approximately 210,000 new cases diagnosed per year worldwide (1). About 80% of the RCC belong to the clear cell RCC (ccRCC) which is commonly characterized by loss of 1 short arm of chromosome 3 and mutation of the von Hippel-Lindau (*VHL*) tumor suppressor gene on the second short arm of chromosome 3 at position 3p25. The high rate of *VHL* mutations suggests that the inactivation of the multiadaptor VHL protein (pVHL) plays a critical part in ccRCC initiation (2).

Authors' Affiliations: [1]Institute of Surgical Pathology; and [2]Clinics of Urology, University Hospital Zurich, Zurich, Switzerland

Note: Supplementary data for this article are available at Cancer Research Online (http://cancerres.aacrjournals.org/).

Corresponding Author: Holger Moch, Institute of Surgical Pathology, University Hospital Zurich, Schmelzbergstrasse 12, CH-8091 Zurich, Switzerland. Phone: 41-44-255-2500; Fax: 41-44-255-4440; E-mail: holger.moch@usz.ch

doi: 10.1158/0008-5472.CAN-11-0757

The best investigated function of pVHL is its role as a substrate recognition component of an E3 ubiquitin protein ligase complex (3). Under normoxic conditions, pVHL binds the hydroxylated hypoxia inducible factor (HIF)α subunits which leads to their ubiquitination and degradation (4). Under hypoxic conditions or absence of pVHL, the stabilization of HIFα leads to the formation of a heterodimer with HIF1β which initiates enhanced transcription of HIF target genes. Both HIF1α and HIF2α show common but also distinct transcription patterns. HIF1α preferably drives the expression of genes important for apoptotic and glycolytic pathways, whereas HIF2α activates genes involved in cell proliferation and angiogenesis (5–7). Based on these results, it was suggested that HIF2α is more oncogenic than HIF1α. This finding was supported by the observation that silencing of HIF2α in a human *VHL*-negative RCC cell line was sufficient to prevent tumor formation in mice and that HIF2α promotes c-myc activity (8–11). However, recent evidence suggests that HIF1α is responsible for genomic instability which may favor the accumulation of additional genetic hits leading to carcinogenesis (12).

Over 800 *VHL* mutations were identified in both hereditary and sporadic ccRCC (13). More than 50% of these mutations are frameshift and nonsense mutations which are highly likely

to cause loss of pVHL function (14, 15). Because of the large number of missense mutations distributed over the 3 exons of *VHL,* the consequences of such alterations on pVHL's integrity and HIFα stabilization are difficult to predict.

Several studies have been carried out to classify *VHL* mutations identified in the hereditary VHL syndrome (reviewed in ref. 16). Nonsense and frameshift mutations generating *VHL*-null alleles are associated with ccRCC (type 1 VHL disease), whereas type 2 VHL disease is mainly characterized by missense mutations. This type is further subdivided into type 2A (with low risk of ccRCC), type 2B (with high risk of ccRCC), and type 2C which predisposes for pheochromocytoma. Missense mutations affecting pVHL's surface result in a higher risk for developing pheochromocytoma compared with substitutions altering the protein core (17). Forman and colleagues used bioinformatic tools to determine the thermodynamic change (ddG) of missense mutations and linked destabilizing mutations in the interface of HIFα and elongin B to a prevalence of ccRCC, whereas mutations interfering with the elongin C interface resulted in increased risk of pheochromocytoma (18).

Controversial data exist about the prognostic and predictive value of the *VHL* mutation type in sporadic ccRCC. Some groups found a correlation between "loss-of-function" mutations (nonsense and frameshift) and a worse prognosis for patients or higher HIF target-directed response rates, whereas other groups were not able to confirm these results (for review see, ref. 16). A large study at the Dana-Faber Cancer Institute revealed an increased response in ccRCC patients with "loss-of-function" mutations (nonsense, frameshift, and in frame) treated with antiangiogenic therapies (sunitinib, sorefanib, axitinib, or bevacizumab), blocking some of the downstream effects of pVHL (19). In contrast to nonsense, frameshift, and in frame mutations, the impact of missense mutations on the function of pVHL seems to be highly diversified ranging from imperceptable to complete functional loss (20–22).

The goal of our study was to functionally characterize missense mutations in sporadic ccRCC on pVHL and HIF using a combination of *in silico* and *in vitro* assays.

Materials and Methods

Tissue specimens

Two hundred and fifty-six formalin-fixed paraffin-embedded ccRCC samples were histologically reviewed by 1 pathologist (H.M.). This study was approved by the local commission of ethics (ref. number StV 38-2005). Survival time was obtained for 123 patients (48%). The mean age of patients was 64 (31–88), and the mean follow-up of patients was 47 months (0–139). Tumors were graded according to tumor stage (pT) and the Fuhrman grading system and histologically classified according to the World Health Organization classification (23). The histologicl data are listed in Supplementary Table S2.

VHL mutation analysis

For DNA extraction, 3 tissue cylinders (diameter 0.6 mm) were punched from each paraffin block. DNA was extracted according to the QIAGEN EZ1 DNA Tissue protocol for automated purification of DNA from tissue (Qiagen). PCR was carried out as previously described (24) with slight modifications. Only 1 PCR step with 40 cycles was carried out by using unlabelled primers. As mutations are rare in the 5′ region of exon 1, the first 162 coding basepairs of *VHL* were excluded from sequence analysis (25). DNA sequencing was carried out by using the BigDye Terminator v1.1 Cycle Sequencing Kit (Applied Biosystems). The obtained sequences were compared with the National Center for Biotechnology Information (NCBI) sequence AF010238 by using NCBI's Blast 2 Sequences. *VHL* point mutations were validated by a second separate PCR and sequencing analysis.

In silico analysis of *VHL* mutants

Two crystal structures of pVHL in complex with elongin B, elongin C, and the HIF peptides are available (26, 27) and stored in the Piccolo database of protein interaction (PDB codes 1lm8 and 1lqb; ref. 28). As input for *in silico* analyses pVHL was separated from the VHL/elongin C/elongin B complex stored in the piccolo database 1LM8.pdb. Swiss PDB viewer "Deep View v.4.0" (http://spdbv.vital-it.ch) was used to locate the missense mutation either to the surface of pVHL or to its core. A threshold for amino acids (aa) with a solvent accessibility of more than 9% was defined as "surface" (29). To predict the association of disease because of missense mutations, the program Site Directed Mutator (SDM) was used which was developed by the Crystallography and Bioinformatic group from the University of Cambridge (30, 31). SDM calculates the ddG of the protein after 1 missense mutation (32, 33). A ddG of more than 2 is set by the algorithm as a cutoff for a disease-associated mutation. The program Crescendo, which predicts the most essential regions and aa for protein–protein interactions because of conserved regions was used to analyze the impact of missense mutations on protein–protein interactions (34).

Cell culture

Human RCC4 cells negative for pVHL, human telomerase reverse transcriptase-immortalized retinal pigment epithelial cell line (hTERT RPE-1) positive for pVHL19 (kindly provided by Wilhelm Krek, Institute of Cell Biology, ETH Zurich, Switzerland), and mouse embryonic fibroblasts (MEFs) negative for pVHL and p53 (kindly provided by Ian Frew, Institute of Physiology, University of Zurich, Switzerland) were grown in Dulbecco's modified Eagle's medium supplemented with 10% fetal calf serum (FCS) in a humified incubator with 5% CO_2 at 37°C. RCC4 and hTERT RPE-1 cell lines were authenticated by short tandem repeat profiling on March 15, 2011 and April 26, 2011, respectively, which was carried out by Identicell (Department of Molecular Medicine, Aarhus University Hospital Skejby, Aarhus, Denmark). The MEF VHL null/p53 null cell line was generated after SV40 infection for transformation, adenoviral cre recombinase infection for pVHL and p53 knockout, and single cell cloning. MEFs were not authenticated. MEFs were transfected with 1 μg vector by using Fugene6 (F. Hoffmann-La Roche AG) for transient and stable transfection. Stable polyclonal transfectants were

generated by selection with 0.5 mg/mL geniticin/G418 (Invitrogen AG) over 1 month. RCC4 and hTERT RPE-1 cells were transduced in the presence of polybrene (4 μg/mL) with viral supernatant produced by 293Amphopack cells (Clontech-Takara Bio Europe) transfected with *VHL* wild type (WT) or mutants and selected with 4 μg/mL puromycin (Sigma–Aldrich) over 1 month. Dimethyloxalyl glycine (DMOG; Cayman chemical) treatment of generated MEF cell lines was carried out over 24 hours at 1 mmol/L. DMOG experiments were independently repeated twice.

Cloning of *VHL* mutants and HIF reporters

VHL mutants were generated by using the one-step PCR mutagenesis Kit (Agilent Technologies Inc.) and pcDNA3.1-*VHL* including a hemagglutinin (HA) as template. The HIF reporter construct pcDNA3.1-HIF1α-GFP (HIF1α Gene ID: 15251) was kindly provided by Stefanie Lehmann (Institute of Biomedical Engineering, ETH Zurich, Switzerland). pcDNA3.1-HIF2α-GFP (HIF2α Gene ID: 2034) was obtained by PCR amplification of pcDNA3.1-HIF2α and cloned into *Sac*II and *Not*I restriction sites of the pcDNA3.1-GFP vector. All constructs were sequence verified.

pVHL stability assay *in vitro*

RCC4 and hTERT RPE-1 cells stably expressing the control vector, WT *VHL* or *VHL* mutants were grown to 80% to 90% confluency in a 6-well format and then treated with 40 μg/mL cycloheximide (Invitrogen) for different time points (0, 1.5, 3, and 6 hours). Zero hours was taken as reference input for the Western blot analysis. After incubation, cells were harvested, processed, and analyzed by Western blot. Cycloheximide experiments were carried out once for RCC4 WT, RCC4 Ser68Thr, and RCC4 Leu101Pro. Experiments for hTERT RPE-1 VHL WT were carried out 3 times independently and once for hTERT RPE-1 Ser68Thr and hTERT RPE-1 Leu101Pro.

Western blot

Cells were lysed in radioimmunoprecipitation assay buffer supplemented with protease inhibitors (F. Hoffmann-La Roche AG) for 30 minutes on ice. The protein concentration was determined by using the BCA Protein Assay Kit (Thermo Fisher Scientific Inc.). Equal amounts of protein were loaded on a 4% to 12% gradient Bis-Tris gel (Invitrogen) and transferred onto a nitrocellulose membrane (Whatman). Membranes were blocked for 1 hours in 5% milk powder and then incubated with mouse anti-HA (1:1,000 dilution; Invitrogen), rabbit anti-human VHL CT (1:1,000 dilution; kindly provided by Wilhelm Krek), or mouse anti–β-actin (1:1,000 dilution; Chemicon) overnight at 4°C. Subsequently, membranes were incubated with the appropriate secondary antibody for 1 hour at room temperature. Proteins were detected by using the ECL Kit (Thermo Fisher Scientific Inc.).

FACS analysis

Cells were transiently transfected with HIF reporters and harvested after 24 hours with trypsin and washed in PBS for the fluorescence-activated cell sorting (FACS) analysis. The cells were then resuspended in FACS buffer (PBS, 2% FCS) and dispersed through a filter into a FACS tube (BD Bioscience). Cells were kept on ice in the dark until analysis with the FACS Calibur (BD Bioscience). The flow rate was adjusted to 200 to 300 events per second and 10,000 events were measured in total per sample. Data analysis was conducted by using FlowJo (Tree Star, Inc.). All experiments were conducted in triplicate with the exception of the DMOG treatment where 1 experiment was done in a single well transfection format and a second one in duplicate. The error bars in the figures are ± SD.

Statistics

Contingency table analysis, χ^2 correlation tests, Kaplan–Meier curves, and log-rank tests were calculated by using SPSS/PASW 18.0.0. GraphPad Prism 5 was used for Spearman correlation tests and 1-way ANOVA with Bonferroni's Multiple Comparison tests. $P < 0.05$ was considered significant.

Results

VHL mutations in sporadic ccRCC

Sequence analysis of *VHL* in 256 ccRCC cases resulted in 75 (29%) WT and 181 (71%) mutated tumors (Fig. 1). Six tumors had 2 mutations. There were 88 (47%) point mutations, including 1 silent mutation, 13 (7%) splice mutations, and 86 (46%) deletions/insertions. Point mutations were further subdivided into 22 (25%) nonsense and 65 (75%) missense mutations. The deletions/insertions were split into 74 (86%) frameshift and 12 (14%) in frame mutations. All mutations are listed in Supplementary Table S1.

The distributions of nuclear differentiation grade (Fuhrman), tumor stage (pT), and *VHL* mutation type are summarized in Supplementary Table S2. Survival analysis revealed no significant differences neither between WT and mutated *VHL* nor between the different mutation types (Fig. 1B). The same was true when the mutations and the mutation types were subgrouped according to their exon locations.

The distribution and number of the identified mutations and mutation types within the 3 exons of *VHL* are shown in Figure 2A–J. The number of *VHL* mutations was significantly increased in exon 1 compared with exons 2 and 3. The most frequent mutated amino acids (aa) were found at positions 65 (whole dataset and nonsense, respectively; Fig. 2A and B), 135 (frameshift, Fig. 2C), 78 (missense, Fig. 2D), and 76 (in frame, Fig. 2E). A clustering of mutations was detected from aa 65–77 (nonsense), 61–64/131–137 (frameshift), 86–89/111–119 (missense), and 66–76 (in frame).

In silico characterization of *VHL* missense mutations and protein structure

In a first step, we characterized the *VHL* missense mutations identified in our set of sporadic ccRCC by using the Swiss PDB viewer "Deep View v.4.0." This program predicts whether the locations of missense mutations are pVHL surface or core related. With a threshold of accessibility of the aa of more than 9% (defined as surface; ref. 29), we obtained the most surface mutations in exon 3 ($n = 14$), whereas the majority of the missense mutations in exons 1 ($n = 25$) and 2 ($n = 16$) were

assigned to the core (Fig. 3A). Calculating the surface to core ratio in pVHL (aa 53–213) resulted in similar values for exons 1 (1.9) and 2 (1.7) but a higher value for exon 3 (5.6). This suggests an increased probability of having surface mutations in exon 3. Because of the crystallographic structure of the pVHL complex (pdb code 1lm8), 21 of 23 missense mutations located on the surface of pVHL could be assigned to interact with either HIF, elongin C, or elongin B (Supplementary Table S1, Fig. 3C; ref. 18). The remaining 2 missense mutations were not located in the domain of any known interaction partner. By using the software Crescendo which predicts the most essential regions and aa for protein–protein interactions, most of the missense mutations were also allocated to these conserved regions. Other binding partners (reviewed in ref. 35) listed in Supplementary Table S1 were found to be influenced by the surface missense mutations (Trp88Cys: aPKC, Tyr98-Asn: aPKC/CollIV/CARD9/SP1/KIF3A; Tyr112Asp: aPKC/CollIV/CARD9/SP1/KIF3A/CCT; Thr124Ala: CCT/aPKC/TD-NEM; Gln132Pro: CCT, Leu158Val: p53, Lys159Asn: p53, Arg161Pro: p53, Arg161Gln: p53).

To predict changes of the pVHL structure because of missense mutations, we used the program SDM. The algorithm calculates the ddG caused by a mutation and output values with a ddG more than 2 are defined as "disease-associated." By calculating the ddG values for all missense mutations, we found 48% predicting a significant impact on the protein structure (ddG > 2) and the remaining 52% having "neutral" mutations (ddG < 2). A significant increased number of missense mutations changing the structure of pVHL was detected in exon 1 followed by exons 2 and 3 (Fig. 3D). When we split surface- and core-related mutations according to their exon locations, we observed "disease-associated" mutations primarily in the core of exons 1 and 2 and on the surface of exon 3 (Fig. 3F).

In vitro characterization of *VHL* missense mutations and protein stability

To verify the predictive power of SDM on the ddG and stability of pVHL, we selected 6 missense mutations of which 4 were assigned disease-associated by protein destabilization

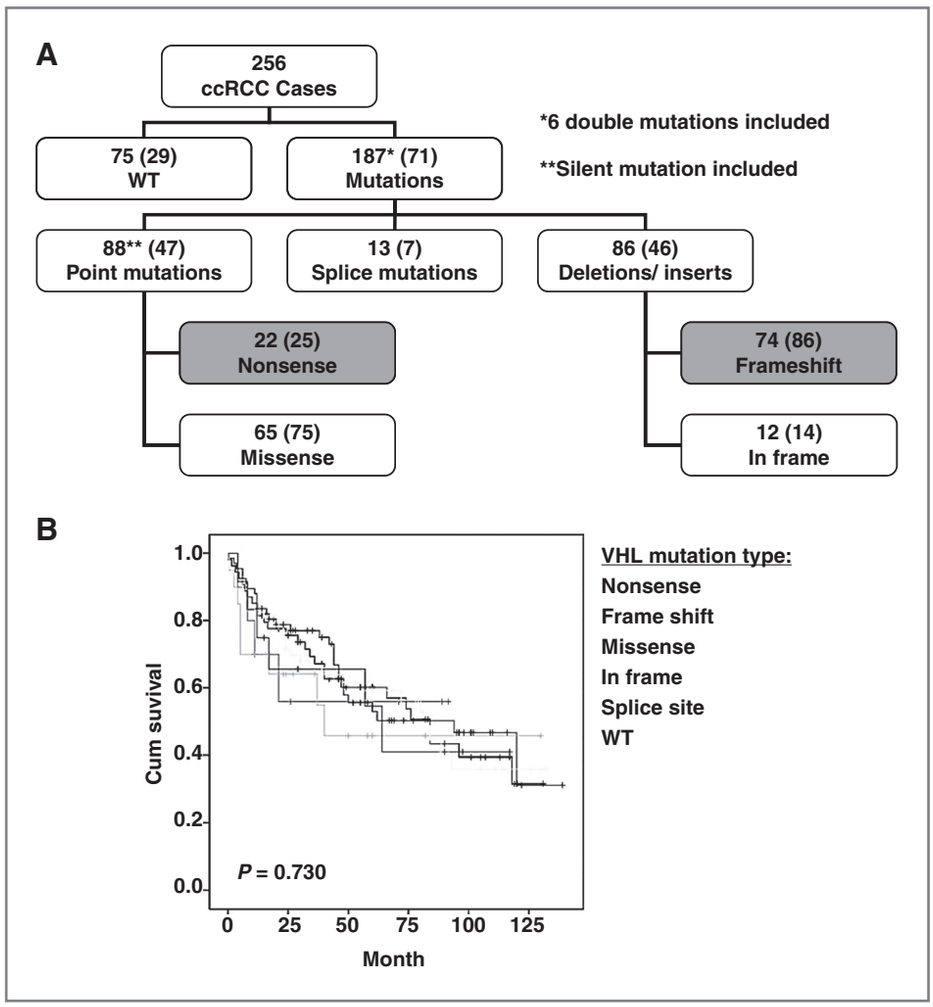

Figure 1. Sequence analysis of *VHL* in sporadic ccRCC. A, DNA was isolated from formalin-fixed tissue and the *VHL* ORF subsequently sequenced which resulted in WT *VHL* and *VHL* with various types of mutations. B, cumulative survival in ccRCC patients with different types of *VHL* mutations.

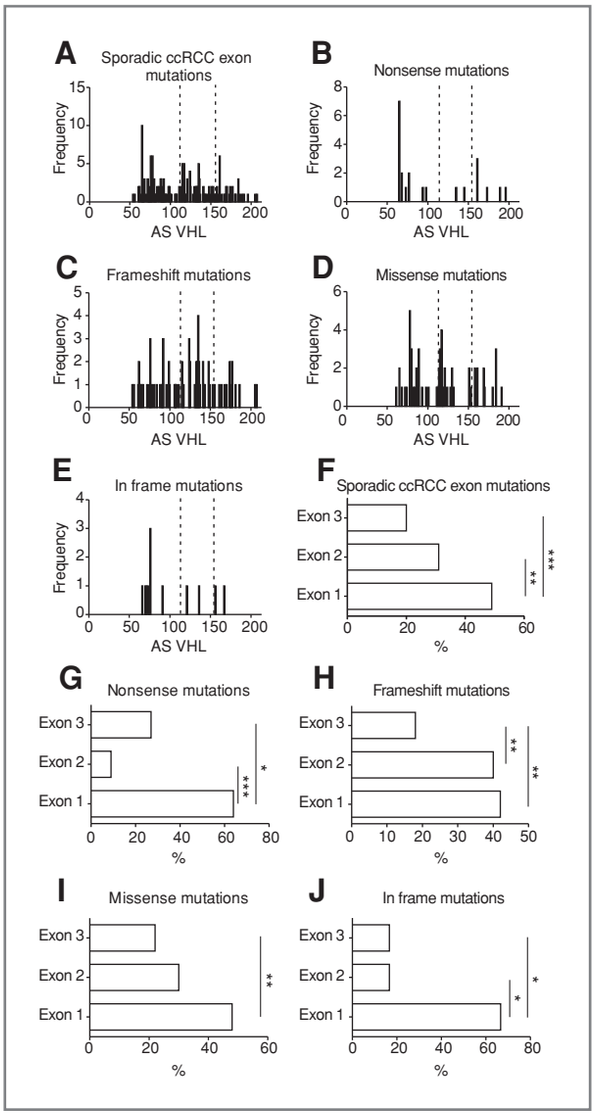

Figure 2. Analysis of the *VHL* mutations. A–E, mutation spectrum and frequency of all, nonsense, frameshift, missense, and in frame mutations found in *VHL* in sporadic ccRCC. Dotted lines represent exon boundaries. F–J, percentage of mutations found after splitting pVHL into its exons 1–3 (*, $P < 0.05$; **, $P < 0.01$; ***, $P < 0.001$). Dotted lines represent VHL exon boundaries.

(Ser68Thr, Gly93Glu, Leu101Pro, and Tyr112Asp), 1 was assigned disease-associated by protein stabilization (Pro86-His), and 1 was neutral (Ser68Thr). Four of these missense mutations (Ser68Thr, Gly93Glu, Leu101Pro, and Tyr112Asp) were stably transduced into the RCC4 tumor cell line and 6 (Ser68Thr, Gly93Glu, Leu101Pro, Tyr112Asp, Pro86His, and Trp117Arg) into the hTERT RPE-1. As expected, transduction of the negative control mutation Leu63fsX67 showed no expression in RCC4 and hTERT RPE-1 cells (Fig. 4A and B). In both cell lines, a pVHL expression pattern was observed after transduction of WT pVHL and the neutral pVHL-mutant Ser68Thr as previously described (36). In contrast, the pVHL mutants Gly93Glu, Trp117Arg, and Leu101Pro, which had the highest destabilizing ddG values of 2.9, 4.3, and 6.1, respectively, showed much lower expression levels with bands between 20 and 30 kDa and additional abundant degradation products below 20 kDa which were not detected with the pVHL WT and the mutation Ser68Thr. The lower expression of the bands in these pVHL mutants were not because of decreased mRNA expression as verified by quantitative reverse transcriptase-PCR analysis (data not shown). The pVHL-mutant Tyr112Asp (ddG = 2.6) was only minimally affected by the mutation underscored by the detection of a faint additional band below 20 kDa compared with pVHL WT. Interestingly, the pVHL-mutant Pro86His (ddG = 2.3) expressed in the hTERT RPE-1 cell line showed an increased band intensity of full-length pVHL (30 kDa) compared with the additional bands between 20 and 30 kDa present in the WT protein which reflects the predicted stabilizing effect of the mutation by SDM.

To further investigate the stability of mutant proteins, a cycloheximide assay was carried out with 2 selected missense mutations. pVHL WT and pVHL-mutant Ser68Thr exhibited similar band intensities after 1.5, 3, and 6 hours cycloheximide treatment, whereas the pVHL-mutant Leu101Pro was clearly less stable (Fig. 4C and D). The bands between 20 and 30 kDa as well as the degradation product at 15 kDa were significantly decreased in intensity already after 1.5 hours in the cell line hTERT RPE-1.

In vitro characterization of *VHL* missense mutations and protein function

To address the question whether the prediction of the stability of pVHL mutants influences its functionality, we set up a screening platform based on MEFs negative for pVHL and p53 ($MEF^{-/-}$). First, we transiently transfected hTERT RPE-1 and $MEF^{-/-}$ with an N terminally HA-tagged *VHL* expressed from the pcDNA3.1 vector by using Fugene6 with a vector DNA ratio 3:1, 3:2, and 6:1. In both cell lines, the expression pattern looked very similar (Fig. 5A). Interestingly, the HA Western blot exhibited only 1 major band at approximately 30 kDa compared with the staining with anti-VHL CT suggesting an N-terminal processing of the full-length pVHL. Next, we tested a set of HA-*VHL*–mutant constructs for transient expression in $MEF^{-/-}$; Fig. 5B]. As expected, the VHL-mutant Leu101Pro with the highest destabilizing value (ddG = 6.1) showed the lowest expression levels similar to those shown in Figure 4A and C. To further establish our screening platform, we stably transfected $MEF^{-/-}$ cells with *VHL* WT and selected 3 independent polyclonal pools (batches 1–3) to determine the batch specific variations (Fig. 5C). After selection, the expression levels of pVHL were similar for batches 2 and 3 and slightly lower in batch 1. Subsequently, we transiently transfected these batches with an HIFα-GFP expression vector and verified the expression by Western blot (data not shown), fluorescent microscopy (data not shown), and by quantitative measurement of expression by flow cytometry (FC; Fig. 5D). Compared with $MEF^{-/-}$ that were stably transfected with a negative control vector, the 3 batches were able to decrease the green fluorescent protein (GFP)

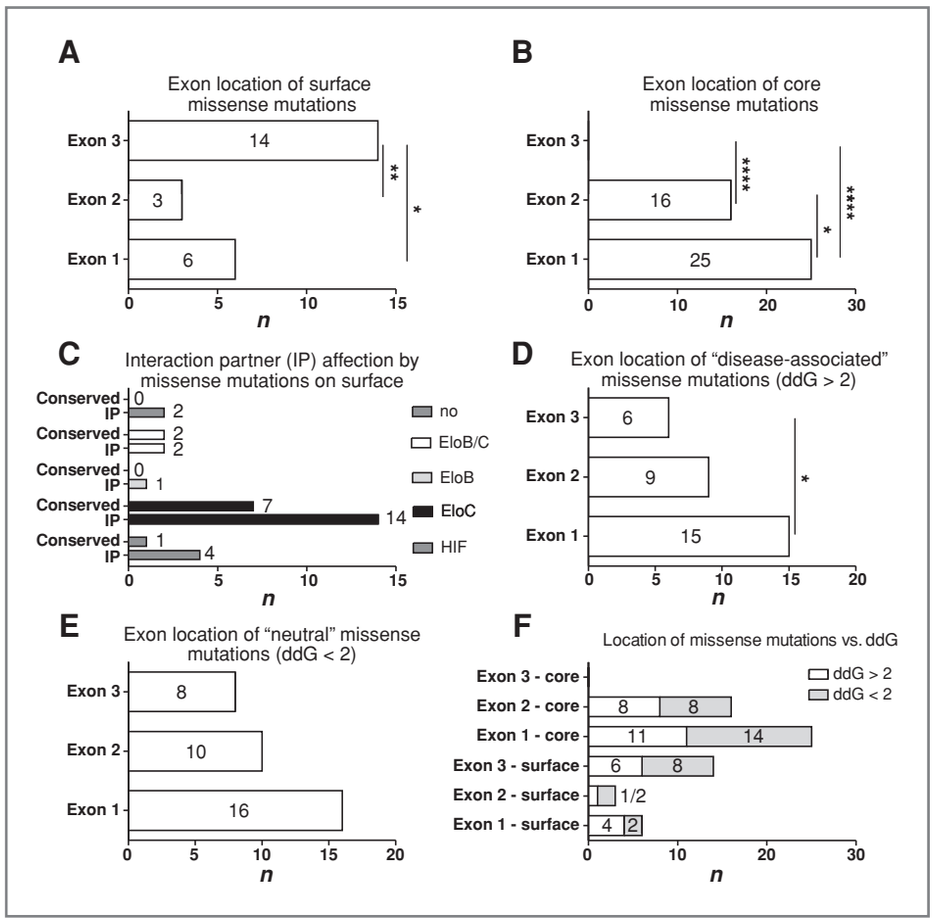

Figure 3. Analysis of *VHL* missense mutations. A and B, *VHL* missense mutations were split according to their exon location in pVHL. Their position was further categorized into surface or core amino acids. C, surface missense mutations were categorized to their location in a specific binding partner domain (EloB = elongin B, EloC = elonginC = C, HIF = hypoxia inducible factor) and their conservation. D, missense mutations were split into exons and the exons further subdivided into the ddG caused by the mutation (ddG > 2 = disease-associated). E and F, deep and surface missense mutations were split into exons and ddG. *, $P < 0.05$; **, $P < 0.01$; ***, $P < 0.001$.

signal by 73%, 63%, and 75%, respectively (Fig. 5E). To validate the system, we added DMOG to $MEF^{-/-}$ pVHL WT cells after transfection with HIFα-GFP and measured the change of the FL-1 channel in gate 1 by FC 24 hours after transfection (Fig. 5F). As a control, pmaxGFP was transfected. After addition of DMOG, the GFP signal increased in both the HIF1α-GFP– and HIF2α-GFP–transfected $MEF^{-/-}$ pVHL WT cells 2.1-fold and 2.2-fold, respectively. DMOG-treated and -untreated $MEF^{-/-}$ pVHL WT cells transfected with pmaxGFP showed no increased GFP signals. Next, we generated $MEF^{-/-}$ stably expressing the same set of pVHL mutants (Fig. 5G) as we used for the transient expression (Fig. 5B). In contrast to the transient transfection experiments (see Fig. 5B), the $MEF^{-/-}$ expressing the pVHL-mutant Leu101Pro showed similar expression levels as pVHL WT.

By using our screening method, we established $MEF^{-/-}$ expressing 29 *VHL* missense mutations, of which 14 have already been described and 15 are not yet registered in the UMD database (13). Additionally, we included 5 well-characterized controls, that is, pVHL WT, Leu63fsX67, Tyr98His, Tyr112His, and Tyr112Asn. $MEF^{-/-}$ Leu63fsX67 was used as negative control and was set to 100% GFP signal for both the HIF1α-GFP and the HIF2α-GFP transfection experiments (Fig 6A and B). pVHL WT was capable of reducing the signal down to 40%. A comparable reduction was obtained with the *VHL* missense mutation Ser68Thr. The ddG of pVHL caused by this mutation was neutral (ddG = 0.44) and not destabilizing. In addition, cycloheximide assays showed that the stability of this mutant was similar to that of the WT pVHL, thus confirming our *in silico* data.

A good correlation was seen between our *in silico* and *in vitro* findings when investigating other missense mutations in our dataset. For example, the pVHL destabilizing missense mutation Leu101Pro (ddG = 6.1) showed a severe loss-of-function represented by a GFP signal of 101% for HIF1α and 95% for HIF2α. It is of note, that the MEF cell line stably expressing pVHL Leu101Pro showed similar expression levels in western blots as pVHL WT (see Fig. 5G). Missense mutations described in VHL disease, such as Asn78Ser (type 1: 102% for HIF1α and 86% for HIF2α), Tyr98His (type 2A: 62% for HIF1α and 55% for HIF2α), Tyr98Asn (type 2B: 77% for HIF1α and 74% for HIF2α), and Ser80Asn (type 2C: 40% for HIF1α and 46% for HIF2α) yielded expected results.

As an additional validation, we also analyzed the impact of *VHL* frameshift mutations on the ability to degrade the 2 HIFα isoforms. For each of the 3 exons we generated 2 frameshift mutations which were identified in our ccRCC patient set. All frameshift mutations except Glu204fsX44, which is located at

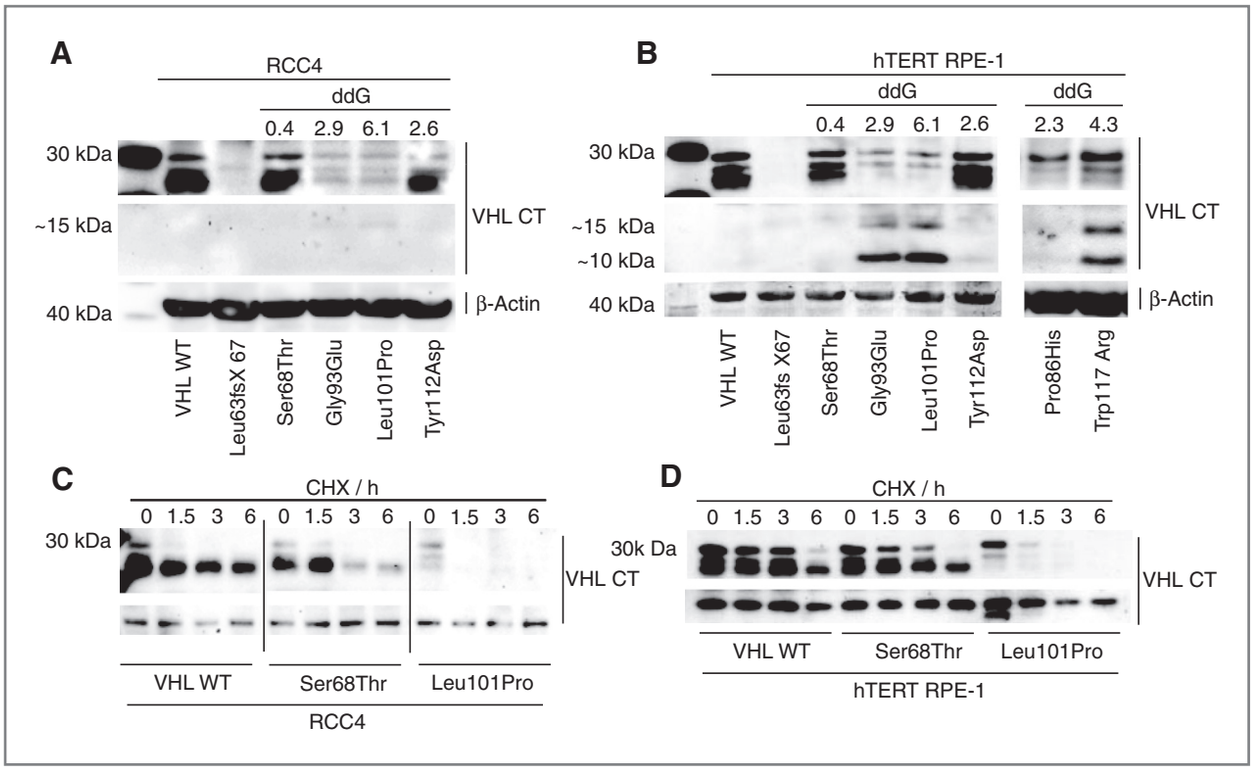

Figure 4. Stability of pVHL mutants. A, RCC4 and B, hTERT RPE-1 cell lines stably expressing pVHL WT, negative control (Leu63fs67X), and indicated mutants with different predicted protein stabilities by SDM (ddG > 2 = disease-associated). The top panel shows staining with anti-human VHL CT with 3 major bands representing intact pVHL, pVHL isoforms, and degradation products. The bottom panel shows the appearance of additional degradation products (10 and 15 kDa) after staining with anti-human VHL CT and longer exposer time. β-actin was used as loading control. C and D, cycloheximide treatment was carried out with cell lines expressing pVHL WT and pVHL mutants Ser68Thr and Leu101Pro with a ddG of 0.4 and 6.1, respectively. Cells were collected at the indicated time points. Anti-VHL CT staining showed the same protein pattern as described in A. An unspecific band was used as loading control.

the very end of exon 3, failed to destabilize HIF1α and HIF2α (Fig. 6C and D). As expected, the frameshift mutations in all 3 exons affected pVHL ability to degrade both HIFα isoforms in the same way (Fig. 6E).

Most of the missense mutations affected HIF1α and HIF2α degradation equally ($r = 0.9208$, $P < 0.0001$). Notably, 3 *VHL* missense mutations showed a selectivity for either HIF1α (Asp121Tyr and Val130Phe) or HIF2α (Asn78Ser) in the range of 10% to 20% (Fig. 6F). Twelve missense mutations identified in our sporadic ccRCC set are also known to be VHL disease related. The analysis of their effects on HIFα destabilization revealed a classification system of *VHL* mutation types that is similar to that described for VHL disease. In sporadic ccRCC, this resulted in missense mutation type 1: HIFα-GFP expression mean 94% (±11%), type 2A: 58% (±3%), type 2B: 83% (±19%), and type 2C: 64% (±24%).

Finally, we correlated the data obtained from pVHL stability prediction and functionality. Spearman correlation coefficient for HIF1α and HIF2α were: $r = 0.5741$, $P = 0.0006$ and $r = 0.5494$, $P = 0.0011$, respectively. A cutoff of 58% of the GFP signal for HIF1α and 54% for HIF2α resulted in 13 disease-associated missense mutations with a ddG more than 2 for each of the HIF isoforms (Fig. 6A and B, boxes A). Eleven (34%) and 16 (50%) mutations were predicted to be "neutral" but were compromised in their ability to ubiquitinate HIF1α and HIF2α, respectively (Fig. 7A and B, boxes B). Only 8 (25%) and 3 (9%) missense mutations were identified with similar functionality on HIF1α and HIF2α destabilization, respectively, as pVHL WT (Fig. 7A and B, boxes C).

Discussion

In this study, we analyzed *VHL* missense mutations in sporadic ccRCC by determining their impact on pVHL's functionality and HIFα stability using *in silico* and *in vitro* assays. The frequencies of the different *VHL* mutation types as well as their distribution over the 3 exons were highly comparable with the results described in previous publications (2, 37).

Our *in silico* approach enabled us to locate missense mutations to the surface or the core of pVHL. Most missense mutations (41 of 64) were located in the core of pVHL. The remaining 23 missense mutations were assigned to the surface of pVHL from which 21 were localized within the binding domains of either HIFα, elongin B, or elongin C. Most missense mutations were located in the elongin C interphase.

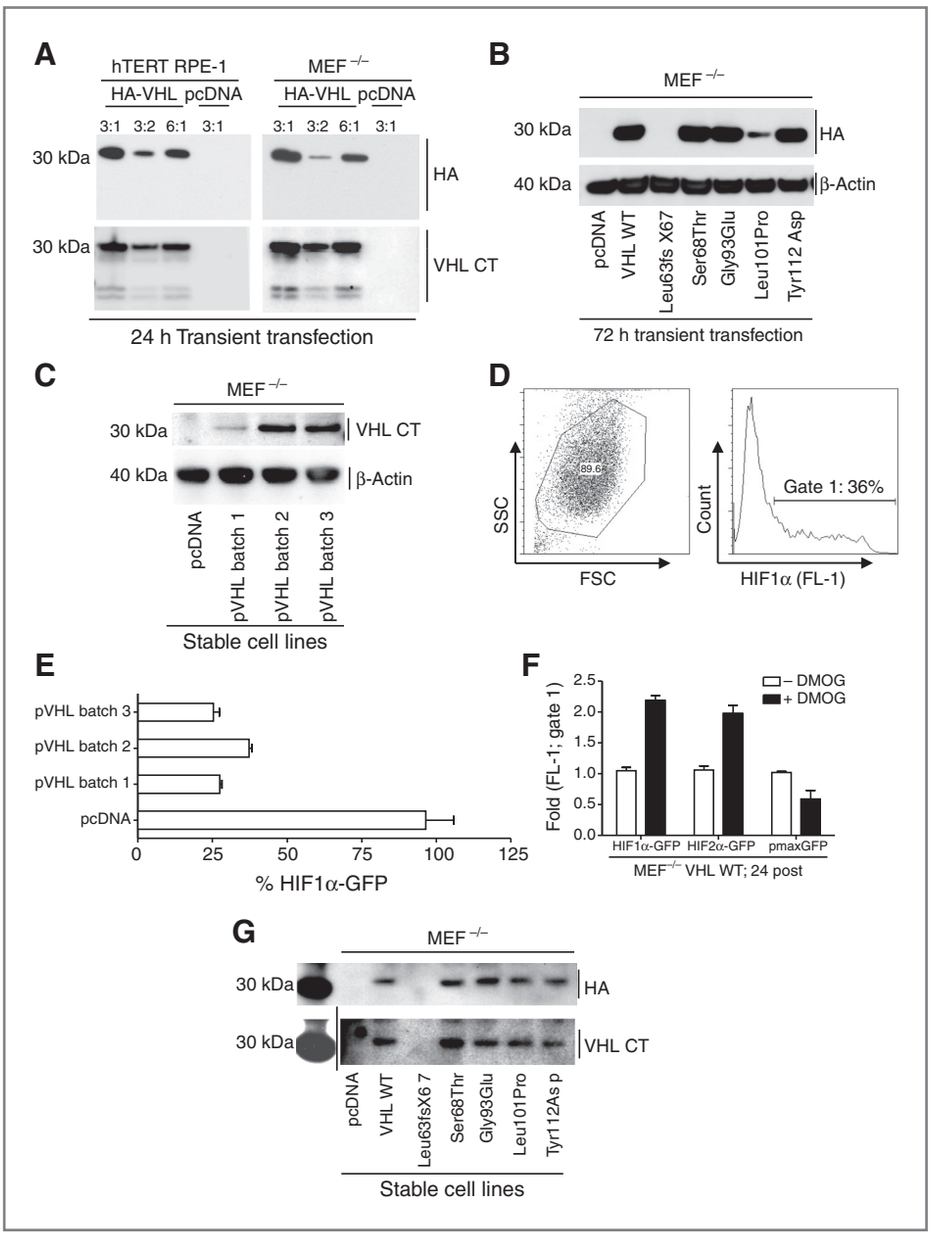

Figure 5. Setup of pVHL functionality screening platform. A, hTERT RPE-1 and MEF$^{-/-}$ were transiently transfected with an N terminally HA-tagged pVHL expressed from the pcDNA3.1 vector by using Fugene6 with a vector DNA ratio 3:1, 3:2, and 6:1. B, transient expression in MEF$^{-/-}$ of selected mutants. C, three polyclonal batches of MEF$^{-/-}$ stably expressing reintroduced *VHL* WT and 1 batch transfected with pcDNA vector were generated. D, FC readout of transient HIF1α-GFP expression in MEF$^{-/-}$ with *VHL*-mutant Leu63fs67X (negative control) was gated first into a life-gate with FSC/SSC. Subsequent analysis of GFP-positive fraction in the histogram resulted in gate 1. E, batches described in Fig. 2A were transfected with HIF1α-GFP and the GFP signal monitored after 24 hours. F, MEF$^{-/-}$*VHL* WT cells were treated with or without DMOG after transient transfection of HIF1α-GFP, HIF2α-GFP, or pmaxGFP and % positive cells counted in gate 1 after 24 hours. G, MEF$^{-/-}$ cell lines stably expressing HA-tagged *VHL* WT, negative control (Leu63fs67X), and indicated mutants.

Interestingly, mutations in the HIFα and elongin B binding sites favoured the formation of ccRCC in VHL syndrome patients, whereas mutations in the elongin C interphase were predisposed to developing pheochromocytoma (18). Surface and core missense mutations were equally distributed in hereditary VHL syndrome patients, whereas in our sporadic tumors 64% of the missense mutations were assigned to the core and 36% to the surface. Notably, over two-thirds of the surface missense mutations analyzed in hereditary RCC were located in the interphase of elongin C (18) which is in agreement with our findings in sporadic ccRCC. We detected an accumulation of mutations in exon 1 where the binding site of HIF is located. In contrast, most mutations of hereditary VHL syndrome patients with ccRCC, retinal angioma, central nervous system hemangioblastoma, and pheochromocytoma were located in exon 3. Therefore, loss of pVHL–HIF interaction is more common in sporadic ccRCC compared with its hereditary form.

To resolve the question whether a missense mutation represents a driver mutation, which generates a growth advantage and thus potentially contributes to tumor formation, Carter and colleagues established a computational method termed Cancer-specific High-throughput Annotation of somatic mutations (CHASM; ref. 38). This approach is a powerful tool to analyze missense mutations in multiple genes especially when structures of their gene products are not

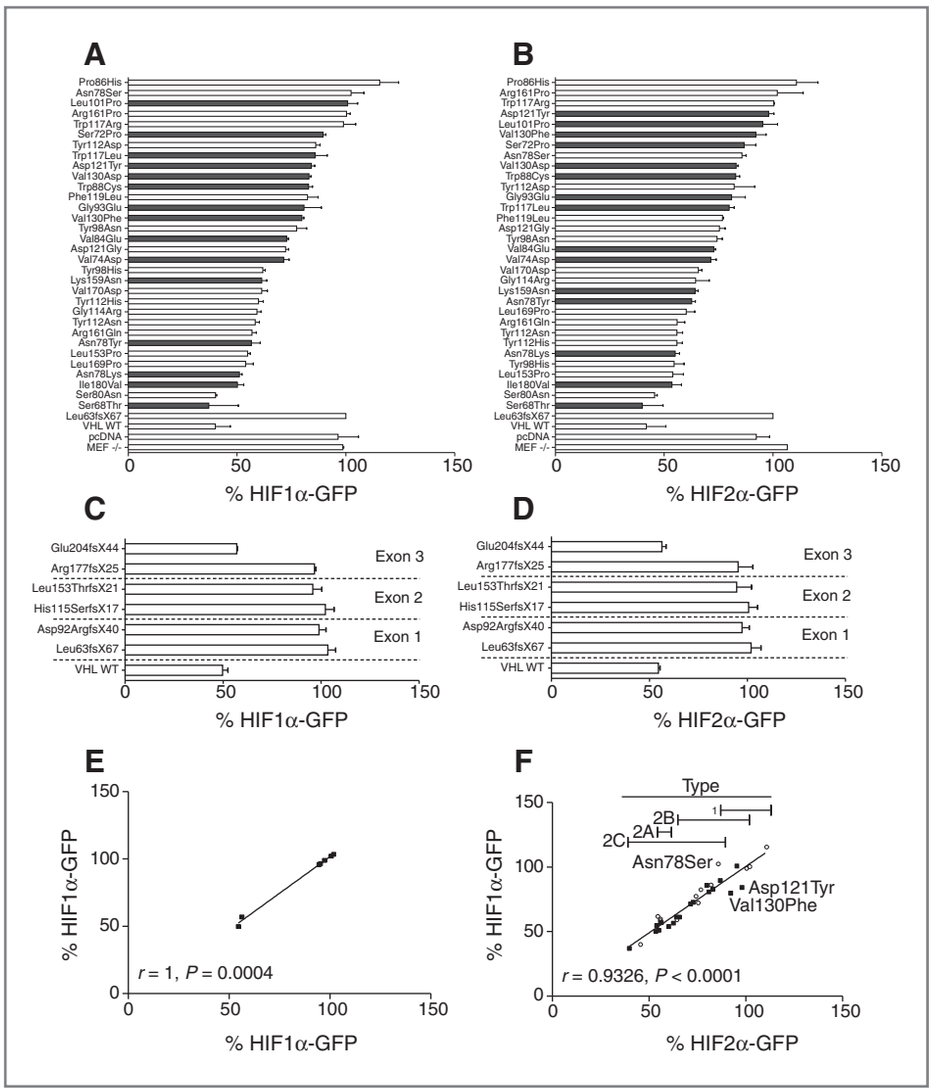

Figure 6. Influence of pVHL mutants on the destabilization of HIFα isoforms. A, MEF pVHL-negative/p53-negative cell lines stably expressing HA-tagged pVHL with various missense mutations were transiently transfected with pcDNA3.1-HIF1α-GFP and GFP expression measured 24 hours later with FC. The pVHL-mutant Leu63fs67X (negative control) was set to 100% for each replica. Black bars represent missense mutations not registered in the UMD database. B, same as in (A) but transfection with pcDNA3.1–HIF2α fusion. C, same as in (A) but with HA-tagged pVHL with various frameshift mutations. D, same as in (B) but with HA-tagged pVHL with various frameshift mutations. For (A–D), experiments were conducted in triplicates. Error bars are ± SDM. E, correlation of HIF1α-GFP and HIF2α-GFP signal in MEF$^{-/-}$ expressing the *VHL* frameshift mutations presented in Fig. 6C and D. F, correlation of HIF1α-GFP and HIF2α-GFP signals in MEF$^{-/-}$ expressing the *VHL* missense mutations presented in Fig. 6A and 6. Open circles represent missense mutations registered in the UMD database as VHL disease causing. Bars represent the range in which the specific VHL disease type was detected.

available. Because of the fact that the crystal structure of the pVHL/elongin B/elongin C complex is known, we used an algorithm which calculates the structural change caused by a specific missense mutation in this complex. Assuming that loss of pVHL function increases HIF transcriptional activity leading to tumor formation and progression, we have considered defining mutations with high structural changes as driver mutations. By calculating the thermodynamic stability of pVHL, we obtained 30 destabilizing driver ("disease-associated") and 32 (excl. 1 silent mutation) passenger ("neutral") mutations. Most of the driver missense mutations were located in exon 1 suggesting that the majority of *VHL* missense mutations in exon 1 predispose to ccRCC by affecting whole protein stability rather than disrupting binding to interaction partners. Only 38% of missense mutations in exon 3 were predicted to destabilize the whole protein structure. However, previous publications reported that loss of elongin binding to pVHL also leads to instability and rapid degradation of the protein (39–41). As all passenger surface-specific missense mutations in exon 3 localized to either elongin C or B, it cannot be excluded that at least some of these mutations exert compromising effects to the regulation of HIF. Interestingly, a recent publication showed that although the missense mutation Arg167Gln causes loss of pVHL–elongin interaction, the HIFα ubiquitination was still functional (22). The authors suggested the formation of a remnant protein E3 ligase complex which is still partially capable of regulating HIF.

To analyze the impact of *VHL* missense mutations on the thermodynamic stability and HIF regulation in more detail, we established an *in vitro* screening platform based on MEFs negative for pVHL and generated polyclonal stable cell lines expressing various pVHL mutants. We used MEFs because higher transient transfection efficiencies are obtained in comparison with pVHL-negative RCC4 or 786-O cell lines. We carried out all experiments by using polyclonal batches with similar levels of pVHL rather than individually picked

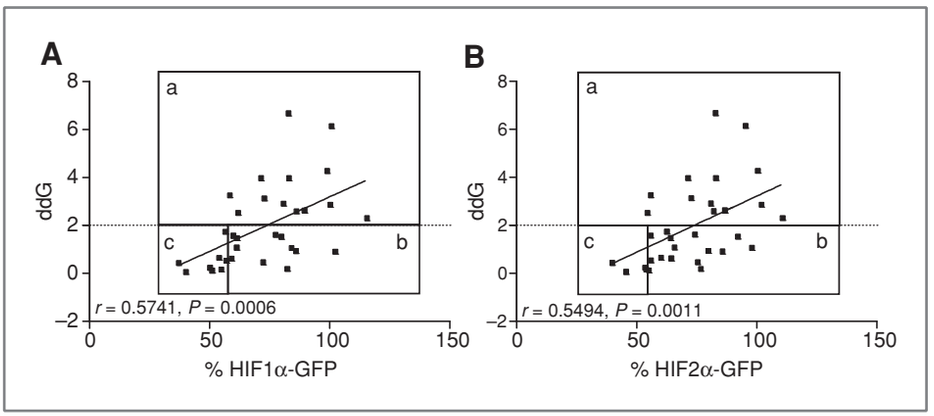

Figure 7. Correlation of pVHL stability and functionality. HIF GFP isoform signals were correlated to the ddG of mutated pVHL (ddG). GFP signals of disease-associated pVHL mutants with ddG more than 2 are in box a. Box b represents *VHL* mutations not predicted to be "disease-associated" by instability but with decreased ability to degrade HIFα. Box c shows *VHL* mutations with a functionality similar to *VHL* WT.

clones to avoid any possible selection for a specific cellular background. Our *in vitro* platforms verified the predicted ddG of more than 2 for the 4 selected mutations which resulted in both pVHL degradation and HIF stabilization. Additionally, the bioinformatic approach could also correctly predict the impact of different aa exchanges at the same position. For example, the missense mutation at aa Arg161Pro (ddG = −2.86) was completely impaired and could not degrade HIFα, as expected because of structural loss of pVHL, whereas the passenger mutation Arg161Gln (ddG = −0.54) retained 56% functionality.

In the majority of the cases in our study, pVHL mutations affected both HIFα isoforms equally. Only 3 missense mutations seem to selectively influence HIF1α and HIF2α stability. However, whether these relatively modest differences are sufficient to significantly influence the tumor behavior remains elusive. A similar result was reported with the mutation Arg167Gln. Hypoxia experiments with murine embryonic stem cells showed that this mutation apparently was able to regulate HIF1α comparable with the WT but not HIF2α (42). This finding was validated by picking several $VHL^{-/-}$ clones transfected with the indicated mutant. In contrast, human 786-O cells stably expressing the same pVHL mutant were able to regulate HIF2α expression upon $CoCl_2$ treatment (22). Similar results were obtained by Bangiyeva and colleagues, who saw comparable HIF2α levels in Arg167Gln, Arg167Trp, and pVHL WT expressing RCC10 cells (21). A contrasting result was published by Clifford and colleagues who detected impaired HIF regulation of both HIF isoforms in RCC4 cells expressing Arg167Gln (43). These different findings may be explained by polyclonal and single cell clone selection, varying levels of exogenous pVHL expression, or by a cell line-specific recruitment of a remnant protein E3 ligase complex.

The majority of the identified *VHL* missense mutations affected both HIFα isoforms. Therefore, it is tempting to speculate that additional factors on the activity (44), translational (45), and stability level selectively influence the expression levels of the HIFα isoforms (7, 10, 11, 46). One prominent class in the stability regulatory network are the oxygen-dependent prolyl 4-hydroxylases (PHD; ref. 47). PHDs hydroxylate both HIFα isoforms at normoxic levels and allow the E3 ubiquitin ligase complex to interact with its substrate. It was suggested that different PHDs influence the levels of HIF1α or HIF2α depending on the cell type, the tissue, and the degree of oxygenation (48–51) which is independent of the *VHL* mutation status.

Our *in silico* tool was able to group *VHL* missense mutations. The used algorithm proved to be a good predictor of pVHL functionality in terms of thermodynamic stability changes. By combining the results from our *in silico* and *in vitro* analyses, we obtained 3 different groups of missense mutations which (i) lead to a severe destabilization of pVHL; (ii) have no destabilizing effects on pVHL but affect the interaction with HIFα, elongin B, and elongin C; and (iii) have functionalities comparable with the WT protein. The first 2 groups represent driver mutations, whereas the latter one consists of passenger mutations. It is to note that 11 and 16 of 32 missense mutations predicted *in silico* to be "neutral" were compromised in their ability to ubiquitinate HIF1α and HIF2α, respectively. The higher number of missense mutations leading to HIF2α stabilization suggests a more specific binding of pVHL and HIF2α. Taken together, these results imply a gradient effect of *VHL* missense mutations on HIF regulation which may be caused by a combination of structural changes and alterations of the binding capability to interaction partners. Our systematic approach enabled us to group these *VHL* mutations according to their effects on HIF which may have important implications for tumor behavior or response to therapy. However, the translation of the HIF (de)stabilizing impact of a *VHL* missense mutation into clinical application needs further investigation.

Survival analysis of *VHL* WT, *VHL* mutation types, and subgrouping of *VHL* missense mutations into predicted destabilizing and neutral missense mutations, showed no differing effects on patient outcome. Our findings are in line with those described in a previous study (2) in which the impact of *VHL* mutation types on patient survival was also investigated. Based on these results, it is tempting to speculate that the analysis of *VHL* mutations in ccRCC patients may serve as predictive rather than as prognostic tool.

In summary, the DNA sequence analysis of *VHL* in sporadic ccRCC identified known and not yet described *VHL* mutations. In addition, our *in silico* and *in vitro* analyses enabled us to classify *VHL* missense mutations into 3 different functional subgroups. The knowledge of the impact of a *VHL* missense mutation on pVHL and HIF stability helps to distinguish between driver and passenger mutations. In this scenario, assessment of the pVHL inactivation status may be useful in predicting response to HIF-targeted drugs.

Disclosure of Potential Conflicts of Interest

No potential conflicts of interest were disclosed.

Acknowledgments

We thank Sonja Brun-Schmid and Roger Santimaria (Institute of Surgical Pathology, University Hospital Zurich, Switzerland) for technical assistance and Carsten Danzer (Cell Biology, ETHZ, Switzerland) for helpful discussions.

Grant Support

This work was funded by the Swiss National Science Foundation and the Zurich Cancer League.

The costs of publication of this article were defrayed in part by the payment of page charges. This article must therefore be hereby marked *advertisement* in accordance with 18 U.S.C. Section 1734 solely to indicate this fact.

Received March 8, 2011; revised June 6, 2011; accepted June 21, 2011; published OnlineFirst June 29, 2011.

References

1. Cancer Mondial. International Agency for Research on Cancer, World Health Organization, Lyon, France. Available from: http://www-dep.iarc.fr.
2. Banks RE, Tirukonda P, Taylor C, Hornigold N, Astuti D, Cohen D, et al. Genetic and epigenetic analysis of von Hippel-Lindau (VHL) gene alterations and relationship with clinical variables in sporadic renal cancer. Cancer Res 2006;66:2000–11.
3. Ohh M, Park CW, Ivan M, Hoffman MA, Kim TY, Huang LE, et al. Ubiquitination of hypoxia-inducible factor requires direct binding to the beta-domain of the von Hippel-Lindau protein. Nat Cell Biol 2000;2:423–7.
4. Maxwell PH, Wiesener MS, Chang GW, Clifford SC, Vaux EC, Cockman ME, et al. The tumour suppressor protein VHL targets hypoxia-inducible factors for oxygen-dependent proteolysis. Nature 1999;399:271–5.
5. Hu CJ, Wang LY, Chodosh LA, Keith B, Simon MC. Differential roles of hypoxia-inducible factor 1alpha (HIF-1alpha) and HIF-2alpha in hypoxic gene regulation. Mol Cell Biol 2003;23:9361–74.
6. Raval RR, Lau KW, Tran MG, Sowter HM, Mandriota SJ, Li JL, et al. Contrasting properties of hypoxia-inducible factor 1 (HIF-1) and HIF-2 in von Hippel-Lindau-associated renal cell carcinoma. Mol Cell Biol 2005;25:5675–86.
7. Gordan JD, Simon MC. Hypoxia-inducible factors: central regulators of the tumor phenotype. Curr Opin Genet Dev 2007;17:71–7.
8. Zimmer M, Doucette D, Siddiqui N, Iliopoulos O. Inhibition of hypoxia-inducible factor is sufficient for growth suppression of VHL−/− tumors. Mol Cancer Res 2004;2:89–95.
9. Kondo K, Kim WY, Lechpammer M, Kaelin WG Jr. Inhibition of HIF2alpha is sufficient to suppress pVHL-defective tumor growth. PLoS Biol 2003;1:E83.
10. Gordan JD, Lal P, Dondeti VR, Letrero R, Parekh KN, Oquendo CE, et al. HIF-alpha effects on c-Myc distinguish two subtypes of sporadic VHL-deficient clear cell renal carcinoma. Cancer Cell 2008;14:435–46.
11. Gordan JD, Bertout JA, Hu CJ, Diehl JA, Simon MC. HIF-2alpha promotes hypoxic cell proliferation by enhancing c-myc transcriptional activity. Cancer Cell 2007;11:335–47.
12. Yoo YG, Christensen J, Huang LE. HIF-1{alpha} confers aggressive malignant traits on human tumor cells independent of its canonical transcriptional function. Cancer Res 2011;71:1244–52.
13. The Universal Mutation Database: The VHL Mutations Database. Montpellier, France. Available from: http://www.umd.be/VHL/.
14. Young AC, Craven RA, Cohen D, Taylor C, Booth C, Harnden P, et al. Analysis of VHL gene alterations and their relationship to clinical parameters in sporadic conventional renal cell carcinoma. Clin Cancer Res 2009;15:7582–92.
15. Schraml P, Struckmann K, Hatz F, Sonnet S, Kully C, Gasser T, et al. VHL mutations and their correlation with tumour cell proliferation, microvessel density, and patient prognosis in clear cell renal cell carcinoma. J Pathol 2002;196:186–93.
16. Gossage L, Eisen T. Alterations in VHL as potential biomarkers in renal-cell carcinoma. Nat Rev Clin Oncol 2010;7:277–88.
17. Ong KR, Woodward ER, Killick P, Lim C, Macdonald F, Maher ER. Genotype-phenotype correlations in von Hippel-Lindau disease. Hum Mutat 2007;28:143–9.
18. Forman JR, Worth CL, Bickerton GR, Eisen TG, Blundell TL. Structural bioinformatics mutation analysis reveals genotype-phenotype correlations in von Hippel-Lindau disease and suggests molecular mechanisms of tumorigenesis. Proteins 2009;77:84–96.
19. Choueiri TK, Vaziri SA, Jaeger E, Elson P, Wood L, Bhalla IP, et al. von Hippel-Lindau gene status and response to vascular endothelial growth factor targeted therapy for metastatic clear cell renal cell carcinoma. J Urol 2008;180:860–5; Discussion 5–6.
20. Hergovich A, Lisztwan J, Barry R, Ballschmieter P, Krek W. Regulation of microtubule stability by the von Hippel-Lindau tumour suppressor protein pVHL. Nat Cell Biol 2003;5:64–70.
21. Bangiyeva V, Rosenbloom A, Alexander AE, Isanova B, Popko T, Schoenfeld AR. Differences in regulation of tight junctions and cell morphology between VHL mutations from disease subtypes. BMC Cancer 2009;9:229.
22. Hacker KE, Lee CM, Rathmell WK. VHL type 2B mutations retain VBC complex form and function. PLoS One 2008;3:e3801.
23. International classification of diseases (ICD). World Health Organization, Geneva, Switzerland. Available from: http://www.who.int/classifications/icd/en/.
24. Schraml P, Struckmann K, Hatz F, Sonnet S, Kully C, Gasser T, et al. VHL mutations and their correlation with tumor cell proliferation, microvessel density, and patient prognosis in clear cell renal cell carcinoma. J Pathol 2002;196:186–93.
25. Banks RE, Tirukonda P, Taylor C, Hornigold N, Astuti D, Cohen D, et al. Genetic and epigenetic analysis of von Hippel-Lindau (VHL) gene alterations and relationship with clinical variables in sporadic renal cancer. Cancer Res 2006;66:2000–11.
26. Hon WC, Wilson MI, Harlos K, Claridge TD, Schofield CJ, Pugh CW, et al. Structural basis for the recognition of hydroxyproline in HIF-1 alpha by pVHL. Nature 2002;417:975–8.
27. Min JH, Yang H, Ivan M, Gertler F, Kaelin WG Jr., Pavletich NP. Structure of an HIF-1alpha -pVHL complex: hydroxyproline recognition in signaling. Science 2002;296:1886–9.
28. Worth CL, Bickerton GR, Schreyer A, Forman JR, Cheng TM, Lee S, et al. A structural bioinformatics approach to the analysis of non-synonymous single nucleotide polymorphisms (nsSNPs) and their relation to disease. J Bioinform Comput Biol 2007;5:1297–318.
29. Ferrer-Costa C, Orozco M, de la Cruz X. Sequence-based prediction of pathological mutations. Proteins 2004;57:811–9.
30. Site Directed Mutator: I-Mutant2.0. Thermodynamic database for protein and mutants. Crystallography and Bioinformatic Group, University of Cambridge, Cambridge, United Kingdom. Available from: http://www-cryst.bioc.cam.ac.uk/~sdm/sdm.php.
31. Site Directed Mutator: Mupro. Thermodynamic database for protein and mutants. Crystallography and Bioinformatic Group, University of Cambridge, Cambridge, United Kingdom. Available from: http://www-cryst.bioc.cam.ac.uk/~sdm/sdm.php.

32. Topham CM, Srinivasan N, Blundell TL. Prediction of the stability of protein mutants based on structural environment-dependent amino acid substitution and propensity tables. Protein Eng 1997; 10:7–21.

33. Smith RE, Lovell SC, Burke DF, Montalvao RW, Blundell TL. Andante: reducing side-chain rotamer search space during comparative modeling using environment-specific substitution probabilities. Bioinformatics 2007;23:1099–105.

34. Chelliah V, Chen L, Blundell TL, Lovell SC. Distinguishing structural and functional restraints in evolution in order to identify interaction sites. J Mol Biol 2004;342:1487–504.

35. Frew IJ, Krek W. pVHL: a multipurpose adaptor protein. Sci Signal 2008;1:pe30.

36. Schoenfeld A, Davidowitz EJ, Burk RD. A second major native von Hippel-Lindau gene product, initiated from an internal translation start site, functions as a tumor suppressor. Proc Natl Acad Sci U S A 1998;95:8817–22.

37. Nickerson ML, Jaeger E, Shi Y, Durocher JA, Mahurkar S, Zaridze D, et al. Improved identification of von Hippel-Lindau gene alterations in clear cell renal tumors. Clin Cancer Res 2008;14: 4726–34.

38. Carter H, Chen S, Isik L, Tyekucheva S, Velculescu VE, Kinzler KW, et al. Cancer-specific high-throughput annotation of somatic mutations: computational prediction of driver missense mutations. Cancer Res 2009;69:6660–7.

39. Schoenfeld AR, Davidowitz EJ, Burk RD. Elongin BC complex prevents degradation of von Hippel-Lindau tumor suppressor gene products. Proc Natl Acad Sci U S A 2000;97:8507–12.

40. Kamura T, Brower CS, Conaway RC, Conaway JW. A molecular basis for stabilization of the von Hippel-Lindau (VHL) tumor suppressor protein by components of the VHL ubiquitin ligase. J Biol Chem 2002;277:30388–93.

41. Jung CR, Hwang KS, Yoo J, Cho WK, Kim JM, Kim WH, et al. E2-EPF UCP targets pVHL for degradation and associates with tumor growth and metastasis. Nat Med 2006;12:809–16.

42. Rathmell WK, Hickey MM, Bezman NA, Chmielecki CA, Carraway NC, Simon MC. *In vitro* and *in vivo* models analyzing von Hippel-Lindau disease-specific mutations. Cancer Res 2004;64:8595–603.

43. Clifford SC, Cockman ME, Smallwood AC, Mole DR, Woodward ER, Maxwell PH, et al. Contrasting effects on HIF-1alpha regulation by disease-causing pVHL mutations correlate with patterns of tumourigenesis in von Hippel-Lindau disease. Hum Mol Genet 2001; 10:1029–38.

44. Mahon PC, Hirota K, Semenza GL. FIH-1: a novel protein that interacts with HIF-1alpha and VHL to mediate repression of HIF-1 transcriptional activity. Genes Dev 2001;15:2675–86.

45. Zimmer M, Ebert BL, Neil C, Brenner K, Papaioannou I, Melas A, et al. Small-molecule inhibitors of HIF-2a translation link its 5′UTR iron-responsive element to oxygen sensing. Mol Cell 2008;32:838–48.

46. Gordan JD, Thompson CB, Simon MC. HIF and c-Myc: sibling rivals for control of cancer cell metabolism and proliferation. Cancer Cell 2007;12:108–13.

47. Wenger RH, Camenisch G, Stiehl DP, Katschinski DM. HIF prolyl-4-hydroxylase interacting proteins: consequences for drug targeting. Curr Pharm Des 2009;15:3886–94.

48. Appelhoff RJ, Tian YM, Raval RR, Turley H, Harris AL, Pugh CW, et al. Differential function of the prolyl hydroxylases PHD1, PHD2, and PHD3 in the regulation of hypoxia-inducible factor. J Biol Chem 2004;279:38458–65.

49. Minamishima YA, Moslehi J, Padera RF, Bronson RT, Liao R, Kaelin WG Jr. A feedback loop involving the Phd3 prolyl hydroxylase tunes the mammalian hypoxic response *in vivo*. Mol Cell Biol 2009;29:5729–41.

50. Metzen E, Stiehl DP, Doege K, Marxsen JH, Hellwig-Burgel T, Jelkmann W. Regulation of the prolyl hydroxylase domain protein 2 (phd2/egln-1) gene: identification of a functional hypoxia-responsive element. Biochem J 2005;387:711–7.

51. Stiehl DP, Wirthner R, Koditz J, Spielmann P, Camenisch G, Wenger RH. Increased prolyl 4-hydroxylase domain proteins compensate for decreased oxygen levels. Evidence for an autoregulatory oxygen-sensing system. J Biol Chem 2006;281:23482–91.